JOURNAL OF APPLIED ELECTROCHEMISTRY **29**: 177–183, 1999.

Influence of silver on electrochemical and corrosion behaviours of Pb–Ca–Sn–Al grid alloys Part II: A.c. impedance and scanning electron microscopy studies

S. ZHONG, J. WANG, H. K. LIU, S. X. DOU

Institute for Superconducting & Electronic Materials, University of Wollongong, NSW 2522, Australia

M. SKYLLAS-KAZACOS

School of Chemical Engineering and Industrial Chemistry, University of New South Wales, Australia

Received 23 September 1997; accepted in revised form 30 June 1998

The influence of silver, in the range of 0.02 to 0.07 wt %, on the electrochemical and corrosion properties of Pb–Ca–Sn–Al grid alloy in sulphuric acid solutions at room temperature was investigated by electrochemical impedance spectroscopy (EIS) and scanning electron microscopy (SEM). EIS was used to study the effect of silver on the surface layer(s) of an electrode under different conditions, while the oxide layers produced on the working electrode surface were examined by SEM. The addition of silver in the alloy inhibits the reactions of Pb to $PbSO_4$ and $PbSO_4$ to PbO_2 and produces a more dense oxide layer which could enhance the corrosion resistance of the alloy.

Keywords: *corrosion*, *grid alloy*, *lead–acid batteries*, *silver*

1. Introduction

The primary properties of interest in grid alloys for lead–acid batteries are the mechanical strength and the corrosion resistance, as well as the compatibility with the active materials (adherence), castability and electrochemical properties. Pb–Ca alloys were proposed as grid alloys as early as 1935 [1]. However, extensive research has been reported since the 1970s [2]. These alloys, due to the high hydrogen and oxygen overpotentials, are commercially used in the new generation of valve-regulated lead–acid batteries (VRLABs). Although the tensile strength of cast Pb–Ca and Pb–Sb alloys are similar, the creep strength of cast Pb–Ca alloys is much lower than that of their antimony counterparts. Pb–Ca alloys have a tendency for nonuniform corrosion due to preferred grain boundary attack. This leads to a swelling effect in the material due to growth of intergranular corrosion products which gives rise to an apparent 'growth' of positive grids in service. Because creep strength is closely correlated to grid growth, Pb–Ca type alloys suffer more severe positive-grid growth in service than Pb–Sb alloys [3]. There has been a series of studies that have involved the improvement of the mechanical properties (especially in the creep strength) and the corrosion stability of Pb–Ca alloys by further addition of alloying elements [4]. Silver is one of the most attractive of these grid alloying elements, with claims that it can improve both the corrosion stability and the creep strength particularly at elevated temperature and even at a comparatively low concentration of 0.01 to 0.1 wt % [5]. Various mechanisms of alloying Ag to Pb and Pb alloys have been proposed which consider either electrochemical properties or microstructure.

The present study reports EIS and SEM studies of silver addition effect on the corrosion behaviour of the conventional Pb–Ca–Sn–Al grid alloy. A progressive thickening of the $PbSO_4$ surface layer formed in 0.5 M H_2SO_4 electrolyte. The oxide layers produced on the working electrode surface under different conditions were examined by SEM.

2. Experimental details

The preparation of sample alloys and working electrodes, the electrode surface treatment and the experimental set-up were described previously [6]. A nominal alloy composition of Pb–0.09 wt % Ca–0.5 wt % Sn–0.02 wt % Al, was chosen as the base alloy. Ag (Aldrich Chem. Co. 99.99%) was added to the molten alloy at about 400 °C under argon protection. The Ag content in the four group sample alloys was: 0, 0.02, 0.05 and 0.07 (wt %), respectively. EIS measurements were performed with an electrochemical impedance analyser (model 6301 EG & G PAR). Data collection, display and analysis is controlled by the software M398 running on a IBM computer. The morphology of oxide layers produced

on the electrode surface under different anodic potentials and time were examined using a scanning electronic microscope (SEM), Leica, 440.

3. Results and discussion

3.1. *Electrochemical impedance spectroscopy studies*

Electrochemical impedance spectroscopy (EIS) has been already applied in studies of the lead–acid battery system. For example, Hampson and Kelly have measured the impedance of PbO_2 films formed on pure lead and lead–calcium alloys [7]; recently Brinic *et al.* [8] reported the results from EIS measurements on lead and lead–antimony alloys in lead sulphate and lead dioxide potential regions. Simon *et al.* [9] studied the passive layers formed on lead–tin alloys in tetraborate and sulphuric acid solutions by EIS.

The impedance behaviour of an electrode system, that is, the impedance plot in either Nyquist form, Bode form or other, mainly depends on two properties of the system: (i) the electrochemical double layer and (ii) the so-called faraday contribution. These properties are influenced by variables such as the electrode potential, the surface concentrations of reactants, temperature of the electrolyte, layer thickness and conductivity and surface roughness.

Figure 1 shows the effect of electrode immersion time on impedance measurements for a common Pb–Ca–Sn–Al electrode in 0.5 M H_2SO_4 at open-circuit potential. During these measurements the same working electrode was used, the electrode was under open-circuit potential and all other parameters were identical. The only variable was the electrode immersion time in the electrolyte. The impedance values indicate that the electrode surface (film) state changes continuously with immersion time. This may be attributed to the progressive thickening of a lead sulphate layer nucleated on the electrode surface. After the initial build-up of the $PbSO_4$ layer, the reaction continues to occur between the $PbSO_4$ crystallites. When the layer is sufficiently thick the diameter of the high-frequency semicircle becomes very large and the electrode tends to be insulated from the electrolyte solution. This explanation can also be used to interpret the Bode plots in Fig. 2. However, the slope of the low-frequency part of the impedance spectrum is lower than the expected Warburg slope (22.5° for a porous or 45° for a planar electrode).

It was also seen that the slope varies with the electrode immersion time. The impedance spectra tend to exhibit only a capacitive semicircle as the electrode immersion time is prolonged. This can be explained if the ion diffusion occurs at the electrode only when it is first immersed in the electrolyte, and then ceases when the $PbSO_4$ layer forms on the electrode surface and becomes thicker and imperme-

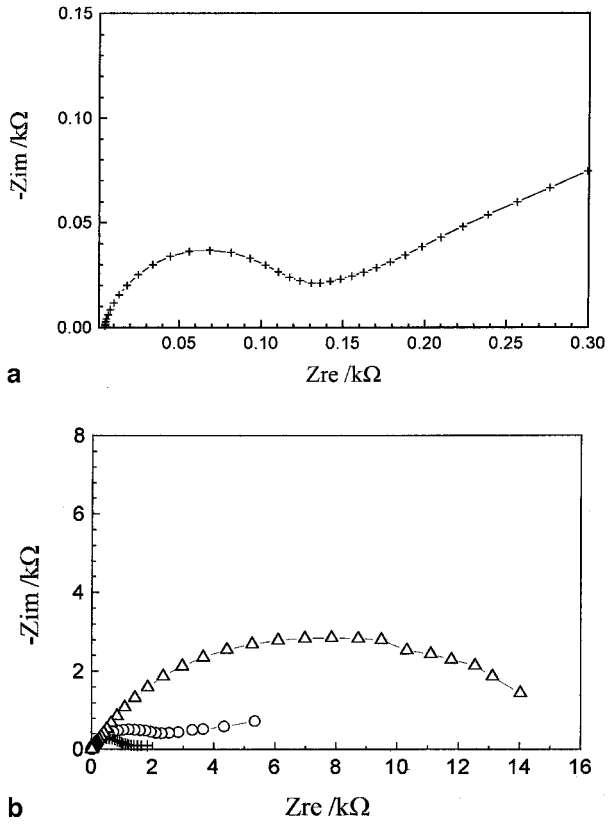

Fig. 1. Nyquist plots for a common Pb–Ca–Sn–Al electrode in 0.5 M H_2SO_4 at the open-circuit potential for different immersion times (a) 1 min (+); (b) 10 min (+), 1 h (○) and 4 h (△), where Z_{re} is the real component of the impedance and Z_{im} is the imaginary component of the impedance.

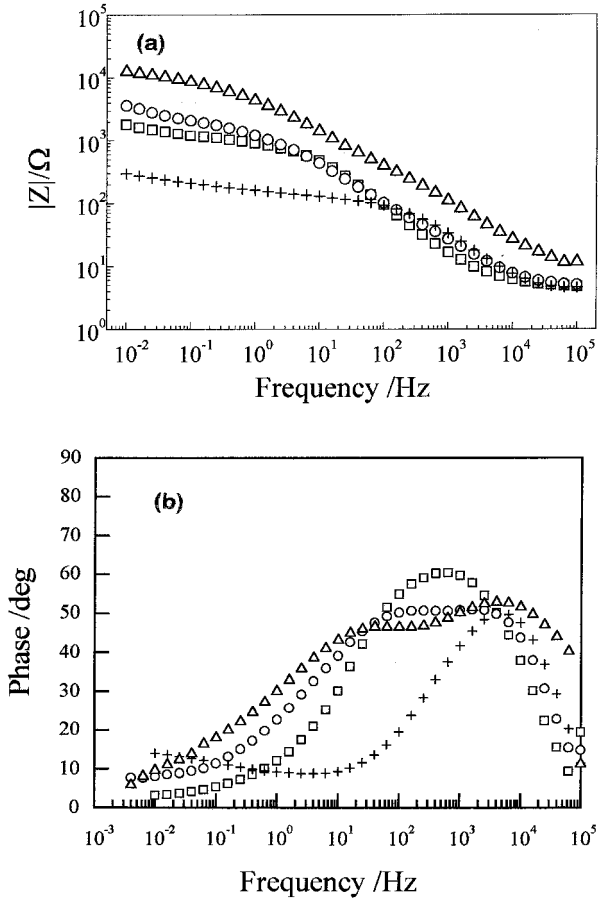

Fig. 2. Bode plots for the same electrode as in Fig. 1, (a) modulus against frequency and (b) phase against frequency. Key: (+) 1 min, (□) 10 min, (○) 1 h and (△) 4 h.

able to ions. It can be concluded from this (Warburg slope) that the electrode reaction under such a condition does not involve the free diffusion of species at the electrode. An equivalent circuit model can be proposed to describe the structure and kinetic changes of the electrode. Furthermore, the proposed equivalent circuit can be mathematically simulated by computer software. For some typical (simple) models, approximate values of most elements in a proposed equivalent circuit can be obtained directly from their corresponding impedance plots and/or by the impedance software.

These treatments were applied in the analysis of the impedance measurements in the present study. It should be pointed out that in the following EIS studies emphasis was given to those cases where kinetic effects are not considered and the properties of the electrode-material system are virtually always assumed to be time-invariant. This assumes that the electrode system approaches steady-state.

Figure 3(a) and (b) show three-dimension impedance plots for the equivalent circuit. In addition to the full response of the 3D plots, Fig. 3(a) and (b) include all three of the different 2D plots. The 3D plots are useful, especially in highlighting experimental errors in the EIS study. Nevertheless, 2D plots are more convenient and more widely used. The following EIS measurements were performed on sample electrodes with different Ag contents in 0.5 M H_2SO_4 solution at 20 °C in the frequency range 100 kHz to 10 mHz. Different potentials were applied which corresponded to different electrode systems.

3.1.1. Electrodes were immersed in the electrolyte under open-circuit potential for 1 h before starting the experiment. The open-circuit potential corresponds to the reversible potential of Pb ↔ $PbSO_4$. Once the electrode reaches steady-state, the Pb/$PbSO_4$/H_2SO_4 electrode system is produced. Nyquist and Bode plots of the different working electrodes are presented in Fig. 4.

According to Pavlov's model [10], only a single $PbSO_4$ layer forms on the electrode under open-circuit potential. To interpret the impedance behaviour, a proposed equivalent circuit model is presented in Fig. 5, where R_{ct} is the charge-transfer resistance, R_L the resistance of the electrolyte, W the mass transport component (Warburg impedance) and C_{dl} the double layer capacitance. In this case, the impedance spectra indicate or the charge-transfer resistance, R_{ct} (or the polarization resistance R_p) and a mass transport component (Warburg impedance, W) in parallel with a double layer capacitance, C_{dl}, as the frequency tends to zero. R_{ct} can be obtained by extrapolation of the semicircle toward the real axis while the electrolyte resistance, R_L, and C_{dl} can be also obtained from Nyquist and Bode plots with impedance software M398 [11]. A schematic diagram for the calculation of the elements in the equivalent circuit is given in Fig. 6.

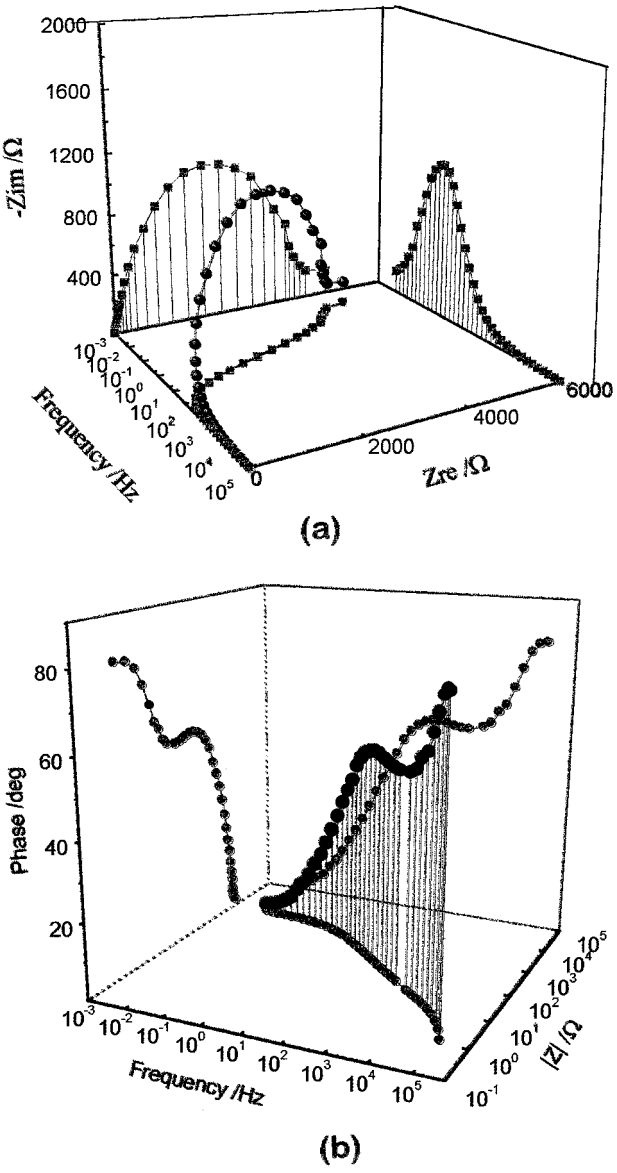

Fig. 3. Three-dimensional plots of an electrode at open-circuit potential (a), and plots for the electrode using modulus and phase angles (b).

Mathematical treatments of the impedance data are also available. The impedance modulus $Z(j\omega)$ can be expressed as a function of frequency $f = \omega/2\pi$ as follows:

$$Z(j\omega) = R_L + \frac{R_{ct} + W}{1 + (j\omega C_{dl}[R_{ct} + W])^{\alpha}} \quad (1)$$

where α is the Warburg coefficient and W is the Warburg impedance which is given by

$$W = \alpha\omega^{1/2}(1 - j) \quad (2)$$

The values of R_L and R_{ct} can be determined from the high and low frequency limits of the measured impedance spectra, respectively:

$$R_L = \lim |Z| \quad (f \to \infty) \quad (3)$$

and

$$R_L + R_{ct} = \lim |Z| \quad (f \to 0) \quad (4)$$

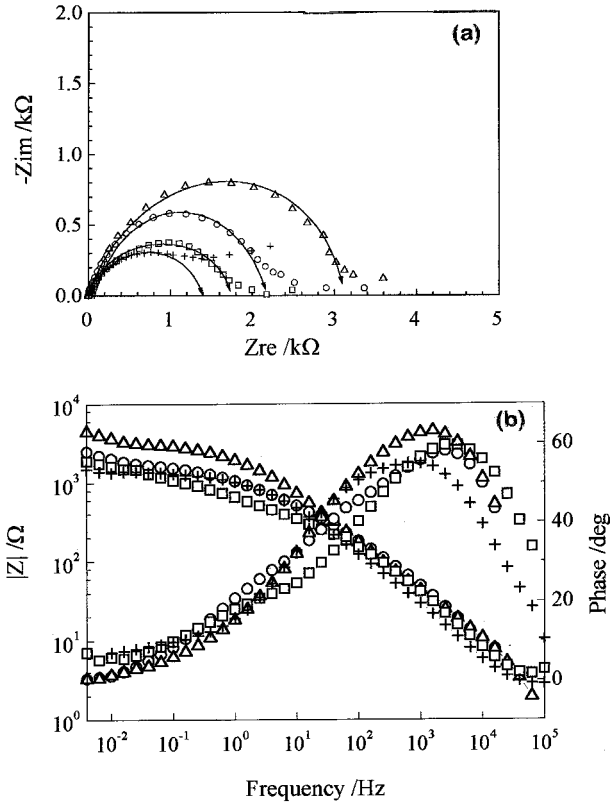

Fig. 4. Nyquist plots (a) and Bode plots (b) for electrodes with different Ag additions at open-circuit potential in 0.5 M H_2SO_4. Key: (△) 0.07 Ag, (○) 0.05 Ag, (□) 0.02 Ag and (+) Pb–Ca–Sn–Al.

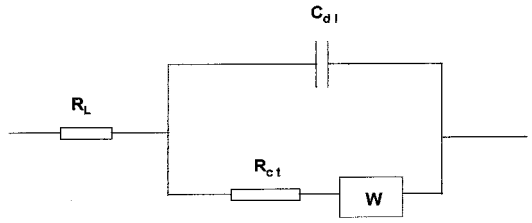

Fig. 5. Equivalent circuit model of the $Pb/PbSO_4$ electrode.

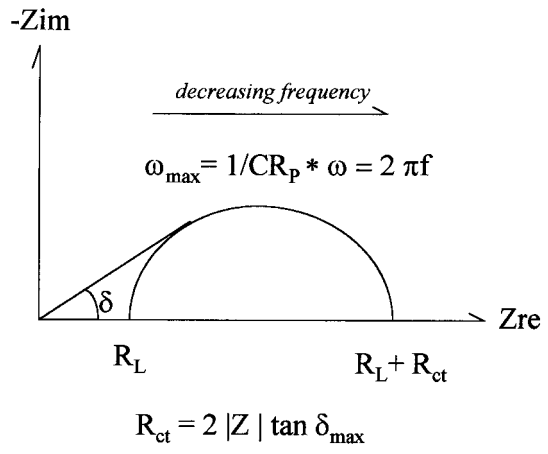

Fig. 6. Schematic diagram for a simple electrochemical system.

Figure 6 presents an electrochemical impedance profile for the above electrochemical system. As indicated, values of R_{ct}, R_L and C_{dl} can be obtained directly from this plot. At high frequencies (Equation 3), only the uncompensated resistance contributes to the real part of the impedance, while at very low frequencies (Equation 4) the charge transfer resistance also contributes. As soon as the excitation waveform becomes much faster than the charge-transfer rate, the electrochemical impedance, (R_{ct}), becomes transparent. The ohmic resistance R_L, on the other hand, represents a constant impedance at all frequencies.

The Nyquist plots of Fig. 4(a) show that the polarization resistance increases, which indicates that the dissolution rate of the $PbSO_4$ film on alloys decreases and the film becomes more stable when the Ag content increases. This result is in agreement with those of earlier anodic polarisation and cyclic voltammetric (CV) measurements [12]. The low values of phase angle in the Bode plots of Fig. 4(b) at low frequencies indicate that no diffusion control occurs under this condition.

3.1.2. Electrodes were anodically polarised at +900 mV for 4 h before starting the experiments. Under this condition, a $PbSO_4$ film is produced first, and a PbO_x layer is formed under the $PbSO_4$ layer. A 'quasi steady state' of the $Pb/PbO_x/PbSO_4$ electrode system is approached after the current has fallen to a negligibly low and constant level. These results are presented in Fig. 7 in Nyquist plots and Fig. 8 in Bode plots.

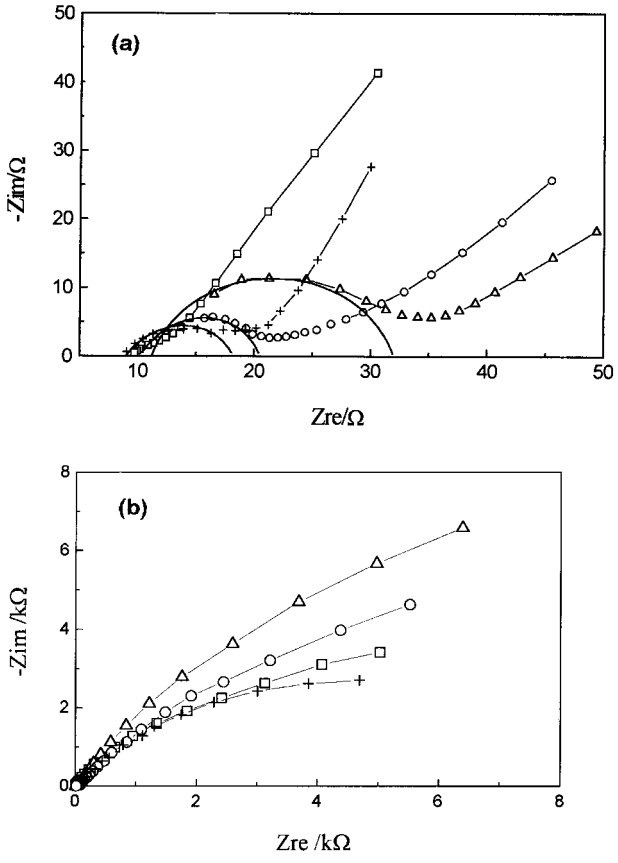

Fig. 7. Nyquist plots for electrodes with different Ag contents at +900 mV: (a) enlarged low frequency parts and (b) overall plots. Key: (△) 0.07 Ag, (○) 0.05 Ag, (□) 0.02 Ag and (+) Pb–Ca–Sn–Al.

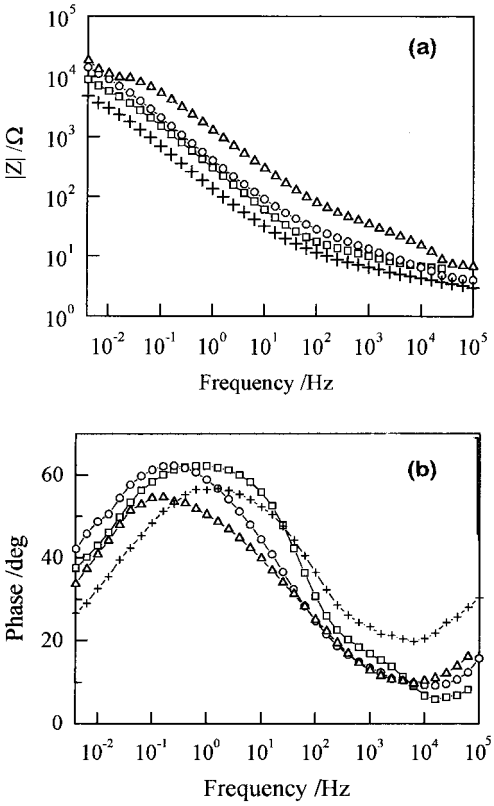

Fig. 8. Bode plots for electrodes as in Fig. 7: (a) modulus against frequency and (b) phase angle against frequency. Key: (△) 0.07 Ag, (○) 0.05 Ag, (□) 0.02 Ag and (+) Pb–Ca–Sn–Al.

The formation mechanism of this two-layer structure has been described by Pavlov *et al.* [13]. When the electrode surface is densely covered with $PbSO_4$ crystals, the size of the intercrystal spaces becomes commensurate with the diameter of the ions in solution. In this case, the pores are penetrated by ions with small ionic radii. Since H^+ and OH^- ions have small radii, while SO_4^{2-} ions are relatively large, their diffusion into the $PbSO_4$ layer is difficult. Thus, the access of SO_4^{2-} ions into the pores is suppressed or eliminated, and the electroneutralization of the positively charged ions there is achieved by OH^- ions, i.e., water in the pores dissociates with H^+ ions migrating to the bulk of the solution and OH^- ions remaining in the pores. The solution in the pores of the $PbSO_4$ layer therefore becomes electroneutral at high pH and the $PbSO_4$ layer is transformed into an ion-selective membrane. According to the potential–pH diagram [14], when pH values reach the neutral or slightly alkaline region, the precipitation of PbO starts. The inner oxide layer (PbO_x, $x = 1 \sim 1.7$) has semiconducting properties and the conductivity of the inner oxide layer depends on the value of x. This duplex structure of $Pb/PbO_x/PbSO_4$ can be described by an equivalent circuit proposed by MacDonald [15], Babić *et al.* [8], and Simon *et al.* [9], which is presented in Fig. 9, where R_1 and C_1 represent the inner layer resistance and capacitance, respectively. R_2 represents the resistance of the outer $PbSO_4$ layer, while C_{dl} represents the capacitance at the double layer.

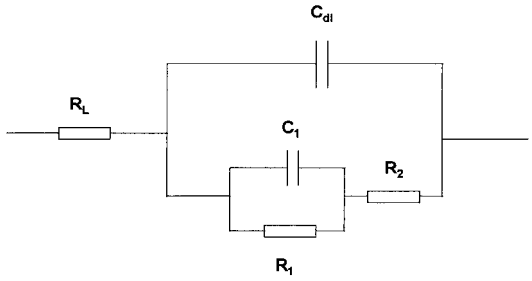

Fig. 9. Equivalent circuit model of $Pb/PbO_x/PbSO_4$ electrode.

Parameters corresponding to the equivalent circuit can be obtained via the simple schematic diagram of Fig. 10 [15]. Semicircles in Fig. 7 show the resistance of the inner layer (PbO layer) is enhanced with Ag additions. This can be attributed to the formation of a high-dispersion intermetallide due to alloying with silver, which increases the compactness of the oxide PbO film and thus causes an increase in the corrosion resistance of the alloy [16].

It may be inappropriate to make quantitative analysis of these equivalent circuit elements and interpret them directly for an electrode system. This is because equivalent distributed elements, such as resistors and capacitors, have simple and ideal physical properties which show exact values in the equivalent circuit, while in a real electrode system these distributed elements depend on many parameters. Therefore, qualitative analysis seems to more appropriate and meaningful. It is also found that different alloying procedures such as different cooling rates employed in the manufacturing procedure will promote different metallurgical structure which will have a strong influence on the impedance spectra. In the present study, consideration was given only to the sample alloys which had identical alloying and casting conditions. Analysis of the impedance data obtained above shows a clear trend of increasing corrosion resistance with the increase in silver content. Although quantitative studies on these impedance data were avoided, qualitative analysis of the above plots via equivalent circuits and corresponding schematic diagrams confirms the results obtained from the earlier anodic potentiodynamic polarization measurements and CV measurements [12].

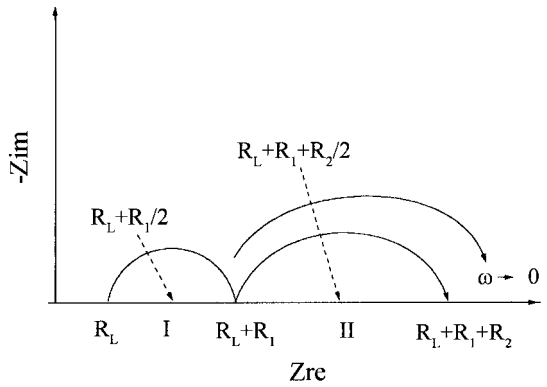

Fig. 10. Schematic diagram to determine element values for the equivalent circuit of Fig. 9 [2].

3.2. *Scanning electron spectroscopy*

The morphologies of the $PbSO_4$ crystals and the oxide layers produced on the working electrode surfaces under different conditions were examined by SEM. These examinations are summarized as follows:

(i) Figure 11(a)–(c) show the SEM images of electrodes which were immersed in a 1.28 relative density H_2SO_4 solution at open-circuit potential for 24 h.

(ii) Figure 12(a)–(c) show the images of electrodes which were anodically polarized at +900 mV (vs Hg/Hg_2SO_4) for 8 h.

The electrodes with different silver contents under condition (i) show similar morphology and range of crystal sizes. Arrows in these photos (Fig. 11) indicate that larger crystals are formed preferably along grain boundaries. Differences in crystal sizes and morphologies between the electrodes with different

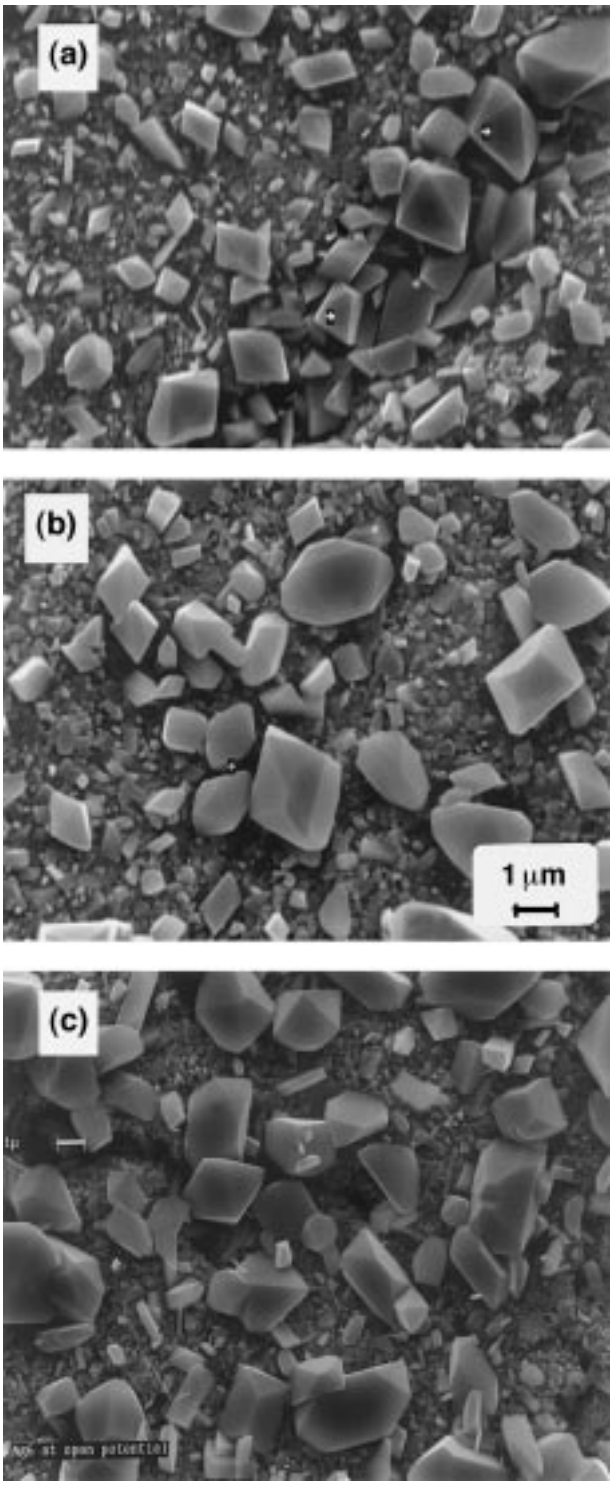

Fig. 11(a)–(c). SEM of electrodes with different Ag contents at open-circuit. Key: (a) 0.02 wt % Ag, (b) 0.05 wt % Ag, (c) 0.07 wt %.

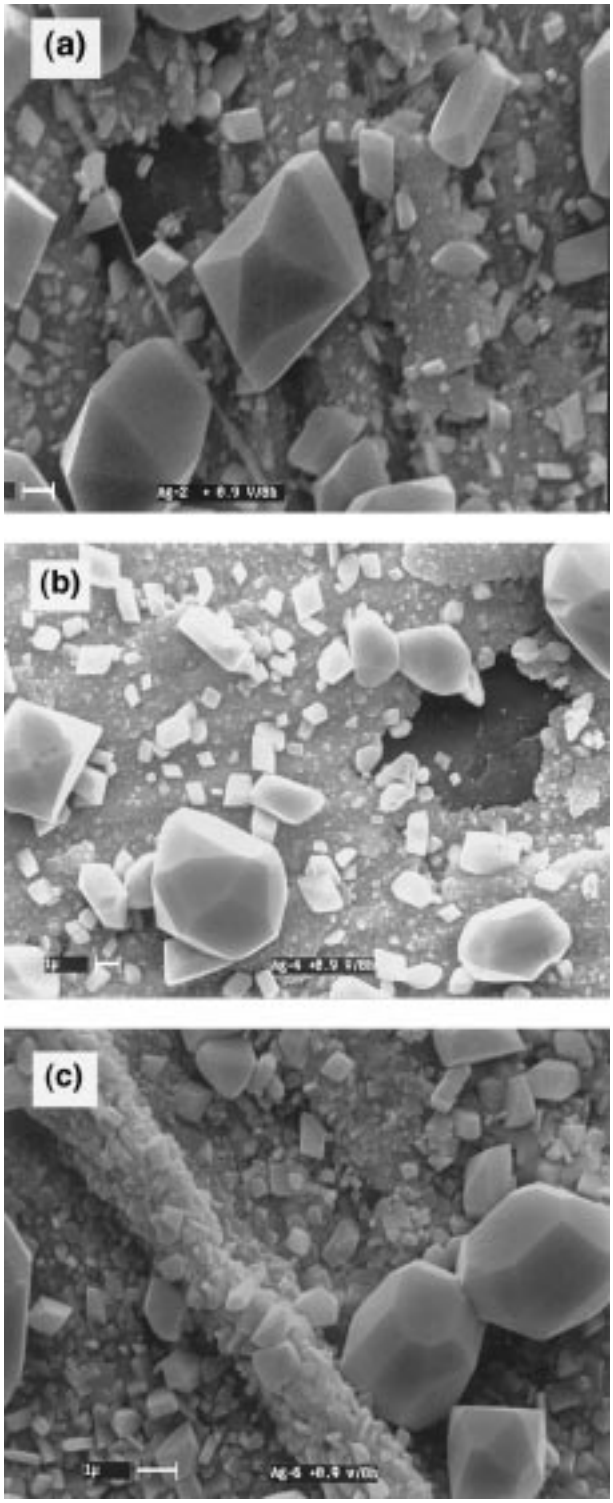

Fig. 12(a)–(c). SEM of electrodes with different Ag contents at +900 mV in 1.28 relative density H_2SO_4 for 8 h. Key: (a) 0.02 wt % Ag, (b) 0.05 wt % Ag, (c) 0.07 wt % Ag.

silver additions under condition (ii) can be seen from Fig. 12.

4. Conclusions

The effect of silver on the mechanical, electrochemical and corrosion properties of a common Pb–Ca–Sn–Al grid alloy has been investigated by different methods. In the present paper EIS and SEM methods were employed while polarisation and CV studies have been reported previously. A number of general conclusions can be drawn from the present and previous studies [12, 17]:

(i) The additions of silver in the composition range studied causes an improvement in mechanical properties. Metallographic examinations on the cross sections of the alloys showed the presence of saw-tooth grain boundaries, which were considered to be responsible for the improved mechanical strength and corrosion resistance.

(ii) From anodic potential dynamic measurements the passive current density was seen to decrease as the silver content is increased. This was attributed to the enhancement effect of silver on the stability of the passive oxide film.

(iii) Cyclic voltammetry showed that silver inhibits the oxidation of $PbSO_4$ (*tet*-PbO) to PbO_2 and the inhibitory effect is proportional to the silver content. The results suggest that the addition of silver to the alloys modifies the energy barrier of PbO_2 formation, thereby enhancing the anodic corrosion stability.

(iv) Gassing properties showed that addition of silver in common Pb–Ca–Sn–Al alloys decreases hydrogen evolution rate and increases the hydrogen overpotential while it enhances the oxygen evolution rate and decreases the oxygen overpotential. This may provide beneficial effects from the viewpoint of gas recombination in VRLA batteries.

(v) From electrochemical impedance spectroscopy and scanning electron microscopy, an influence of the addition of silver on both the kinetics of anodic reaction and the structure of the oxide layers has been shown. In all cases, the electrode impedance reveals that the addition of silver inhibits the reactions of Pb to $PbSO_4$ and $PbSO_4$ to PbO_2.

(vi) SEM examinations show that the effect of silver on the morphology of crystals and oxide layers depends on the electrode potential and time. A higher silver content produces a more dense oxide layer which enhances the corrosion resistance of the alloy.

(vii) The beneficial effect of silver on the corrosion properties of the alloys has been further confirmed by the earlier accelerated corrosion test. These tests showed that the increase in corrosion resistance is non-linearly proportional to silver content. The effect was greatest at a silver content of 0.07 wt %.

References

[1] B. U. Thomas, F. T. Forster and H. E. Harring, *Trans. Am. Electrochem. Soc.* **92** (1947) 313.
[2] N. E. Bagshaw, *J. Power Sources* **33** (1991) 3.
[3] J. Perkings, J. L. Pokorny and M. T. Cole, 'A review of Materialsand Mechanisms which Affect the Performance of Lead–Acid Storage Batteries', Naval Postgraduate School, CA (1976).
[4] N. E. Bagshaw, *J. Power Sources* **53** (1995) 25.
[5] *US Patent 5 298 450* (1994).
[6] S. Zhong, J. Wang, H. K. Liu, S. X. Dou and M. Skyllas-Kazacos, *J. Power Sources* **66** (1997) 107.
[7] N. A. Hampson and S. Kelly, *J. Appl. Electrochem.* **11** (1981) 751.
[8] S. Brinic, M. Metikos-Hukovic and R. Babic, *J. Electrochem. Soc.* **55** (1995) 19.
[9] P. Simon, N. Bui, N. Pebere, F. Dabosi and L. Albert, *ibid.* **55** (1995) 63.
[10] D. Pavlov and N. Iordanov, *J. Electrochem. Soc.* **117** (1970) 1103.
[11] 'Model 398 Electrochemical Impedance Analyzer User's Guide', EG & G Instruments Co. (1993).
[12] S. Zhong, J. Wang, H. K. Liu, S. X. Dou and M. Skyllas-Kazacos, *J. Appl. Electrochem.* **29** (1999) 1–6.
[13] D. Pavlov, 'Power Sources for Electric Vehicles', edited by B. D. McNicol and D. A. J. Rand (Elsevier, 1984).
[14] S. C. Barnes and R. T. Mathieson, *in* 'Batteries 2', edited by D. H. Collins (Pergamon, Oxford, 1965), p. 42.
[15] J. Ross Macdonald, 'Impedance Spectroscope-Emphasizing Solid Materials and Systems' (Jo. Wiley & Sons, New York, 1987).
[16] M. A. Dasyan and I. A. Aguf, 'Current Theory of Lead Acid Batteries' (ILZRO Inc., Technicopy Ltd, 1979).
[17] S. Zhong, H. K. Liu, S. X. Dou and M. Skyllas-Kazacos, *J. Power Sources* **59** (1996) 123.